Available online at www.sciencedirect.com

SciVerse ScienceDirect

Geochimica et Cosmochimica Acta 75 (2011) 7893–7905

Geochimica et Cosmochimica Acta

www.elsevier.com/locate/gca

The energetics of nanophase calcite

Tori Z. Forbes, A.V. Radha, Alexandra Navrotsky *

Peter A. Rock Thermochemistry Laboratory and NEAT ORU (Nanomaterials in the Environment, Agriculture, and Technology Organized Research Unit), University of California, Davis, CA 95616, USA

Received 16 March 2011; accepted in revised form 10 August 2011; available online 28 September 2011

Abstract

Calcium carbonate ($CaCO_3$) is an important component of the near-surface environment. Understanding the nature of its precipitation is important for a variety of environmental processes, as well as for the geologic sequestration of anthropogenic carbon dioxide. Calcite is the most thermodynamically stable bulk polymorph, but energy crossovers may exist that could favor the precipitation of vaterite or aragonite with decreasing particle size. The purpose of this study is to determine the surface energy of calcite, which is the first step towards understanding the effect of particle size on thermodynamic stability in the calcium carbonate system. The enthalpies of five well-characterized calcite samples (four nanophase and one bulk) were measured by acid solution isothermal and water adsorption calorimetric techniques. From the calorimetric data, the surface energies of calcite were determined to be 1.48 ± 0.21 and 1.87 ± 0.16 J/m^2 for hydrous and anhydrous surfaces. These values are similar to those measured for many oxides but larger than predicted from computational models for idealized calcite surfaces. The surfaces of synthetic $CaCO_3$ particles contain a range of planes and defect structures, which may give rise to the difference between the experimental and modeled values.
© 2011 Elsevier Ltd. All rights reserved.

1. INTRODUCTION

Calcium carbonate ($CaCO_3$) is a ubiquitous inorganic component of the near-surface environment, occurring in aqueous systems, soils, sediments, and aerosols (Morse et al., 2007). It precipitates in both fresh and saline waters, and can form by biogenic or abiotic means. Three anhydrous crystalline polymorphs exist: calcite, aragonite, and vaterite (Morse et al., 2007). Under ambient temperature and pressure, calcite is the most thermodynamic stable form, but there are only small energy differences (0.5–3 kJ/mol) between the three phases (Plummer and Busenberg, 1982; Wolf et al., 1996, 2000; Baitalow et al., 1998). Consequently, aragonite and vaterite can be precipitated by slight changes in temperature, ionic strength, counter ions, mixing, or presence of organic molecules (Wray and Daniels, 1957; Han et al., 2006; Nebel and Epple, 2008; Gomez-Morales et al., 2010).

The nature of calcium carbonate precipitation is particularly important for the geologic sequestration of anthropogenic carbon dioxide. Deep saline aquifers, consisting of porous sandstones overlain by capping layers of shale or salt, have been proposed as possible repository sites (Matter and Kelemen, 2009). Mineralization of the carbon dioxide by conversion into solid carbonate phases can provide a larger storage capacity and prevent CO_2 leakage through cracks and fissures in the capping material (Kharaka et al., 2008; Ketzer et al., 2009; Matter and Kelemen, 2009). The chemistry of the host rocks suggests that the precipitation of solid calcium carbonate phases is the primary means for CO_2 mineralization (Ketzer et al., 2009; Matter and Kelemen, 2009).

The molecular level understanding of calcium carbonate precipitation is still incomplete. The classical nucleation pathway for calcium carbonate precipitation, i.e. formation of a critical nucleus, followed by stepwise growth of the crystal, is now in question (Meldrum and Sear, 2009).

* Corresponding author. Tel.: +1 319 384 1320.
E-mail address: anavrotsky@ucdavis.edu (A. Navrotsky).

0016-7037/$ - see front matter © 2011 Elsevier Ltd. All rights reserved.
doi:10.1016/j.gca.2011.09.034

Gebauer et al. (2009) found discrepancies between the nominal and measured Ca^{2+} concentrations in a carbonate-rich solution, suggesting that calcium carbonate precipitation begins with the formation of stable prenucleation clusters. The calcium carbonate clusters could then coalesce to form amorphous calcium carbonate and may undergo rearrangement into one of the three anhydrous calcium carbonate polymorphs (Pouget et al., 2009). The formation of stable prenucleation clusters invokes an alternative pathway to the classic nucleation theory.

The energetics of calcium carbonate precipitation has recently been investigated by Radha et al. (2010). A trend in thermodynamic stability is observed from (least stable) hydrous amorphous calcium carbonate → anhydrous amorphous calcium carbonate → vaterite → aragonite → (most stable) calcite. These results indicate that amorphous calcium carbonate could be a precursor to any of the crystalline calcium carbonate phases.

Calcium carbonate precipitation in a geologic repository for CO_2 is further complicated by the nature of the porous sandstone aquifer. First, precipitation reactions could occur in confined micro- and nanopore spaces, suggesting that the particle size will also be in the nanoscale regime (Kharaka et al., 2008). Increasing the surface area of the material (decreasing the particle size), combined with small energy differences between phases, can lead to crossovers in the free energies of the polymorphs, i.e. the order of thermodynamic stability can be inverted (Navrotsky, 2003). These thermodynamic crossovers have previously been observed for several metal oxide systems, including the TiO_2 polymorphs (rutile, brookite, and anatase) (Ranade et al., 2002) and the iron oxide phases (Navrotsky et al., 2008). Similar crossovers for the calcium carbonate system could alter the dominant calcium carbonate phase precipitated in a repository setting. In addition, the increased pressures, temperatures, and ionic strength of the aquifer may change the precipitation pathway and phases (Kharaka et al., 2008).

To increase the molecular-level understanding of the precipitation reactions for calcium carbonate, we are investigating the energetics of the calcium carbonate phases by acid solution and water adsorption calorimetric techniques. The current study focuses on the characterization and calorimetry of nanophase calcite to obtain the surface enthalpy of calcite. The nature of water–calcite interface has been characterized by water adsorption calorimetry using a coupled system of a Micromeritics ASAP2020 analyzer and a Setaram DSC111 Calvet microcalorimeter operated at 25 °C This work constitutes a first step in investigating possible size induced energy crossovers in the calcium carbonate system.

2. EXPERIMENTAL METHODS

2.1. Sample preparation

High purity nanophase calcite is available commercially because of its use in sealants, synthesis of rigid polyvinyl chloride, high strength reinforcement for rubber, nucleating agent in emulsion polymerization, carriers for catalysts, and flow control additives. Four nanophase calcite samples were obtained from different sources: Specialty Minerals, Inc. Bethlehem, PA (sample designation: SM-1), SpringSky Nanomaterials, Houston, TX (SS-1), NanoMaterials Technology Co., Ltd., Shanxi, China (NMT-1), and NanoMaterials Technology Co., Singapore (NMT-2). Samples SM-1, and SS-1 were used as received; NMT-1 and NMT-2 samples were shipped as a paste. The pastes were dried overnight in a vacuum oven set at 100 °C to remove excess moisture and ground into a fine powder with a mortar and pestle.

Bulk calcite was synthesized via a precipitation reaction with $CaCl_2$ (1.912 g in 12.5 mL) and K_2CO_3 (4.839 g in 17.5 mL). The K_2CO_3 solution was slowly added (1 drop/sec) to the $CaCl_2$ solution and then mixed at room temperature for 40 min. The product was filtered and rinsed several times with deionized water and ethanol. The sample was heated in an alumina crucible at 500 °C for 16 h.

2.2. Characterization methods

Phase identification and particle size analysis were performed by powder X-ray diffraction. The samples were prepared by basic front loading techniques and the powder X-ray diffraction patterns (XRD) were collected on a Bruker Advance diffractometer equipped with a LynxEye solid state detector. The patterns were collected from 10° to 90° 2θ with a step size of 0.02° and a time per step of 1 s. LaB_6 was used as an internal standard for specimen displacement corrections. A FWHM curve was constructed using the LaB_6 standard to correct for instrument effects. Phase identification and particle size analysis were performed using the JADE 8.0 software.

The elemental composition of each sample was analyzed by inductively coupled plasma mass spectrometry (ICP-MS). The samples were prepared for analysis by dissolving approximately 1.5 to 2.0 mg of each sample in 50 mL of a 3% HNO_3 (prepared from concentrated nitric acid (EMD Chemicals, NJ, USA, 68–70%, ACS GR) by dilution using 18.2 mohm water). The analyses were performed using an Agilent 7500CE ICP-MS (Agilent Technologies, Palo Alto, CA) by the Interdisciplinary Center for Plasma Mass Spectrometry at the University of California at Davis.

The presence of H_2O, amorphous calcium carbonate, and/or organics was examined by infrared spectroscopy using a Bruker Equinox 55 FTIR spectrometer. KBr pellets containing the powdered samples were run from 400 to 4000 cm^{-1}. Blank subtractions were performed using pure KBr.

Thermogravimetric analysis of each sample was performed on a Setaram Instruments Labsys Evo in air from 30 to 1000 °C with a heating rate of 10 °C/min. The weight loss due to the minor amounts of water present in the samples is difficult to quantify using TGA. Additional heating experiments on gram quantities of sample were performed in a furnace to determine weight loss after the sample was heated to 400 °C for 16 h.

The surface area of the samples was characterized by Brunauer–Emmett–Teller (BET) nitrogen adsorption measurements and transmission electron microscopy

(TEM). The BET surface areas were determined using a Micromeritics ASAP 2020 instrument. Approximately one gram of each sample was degassed for 12 h at 150 °C. A five point N_2 adsorption isotherm was collected in triplicate for all samples. A Phillips CM-12 TEM was used to determine the crystallite size by a third independent method and to observe possible particle aggregation. The TEM was equipped with a tungsten tip and operated with a 100 kV electron beam. Samples were dispersed on lacey carbon Type A 300 mesh copper grids using isopropyl alcohol.

2.3. Calorimetric methods

2.3.1. Acid solution calorimetry

The enthalpies of solution for calcite samples were measured using a CSC 4400 isothermal microcalorimeter (Calorimetry Sciences Corporation) operated at 26 °C with stirring. Five to ten mg of pelletized sample was dropped into 25 g of 5.0 N HCl (Alfa Aesar) and the heat effect (0.1–0.2 J) was recorded over the reaction time. Previous experiments have indicated that the calorimeter in this configuration is capable of detecting effects as small as 0.02 J (Majzlan et al., 2007). The integrated calorimetric curve was converted to the enthalpy of solution (ΔH_{sol}) using a calibration factor obtained by dissolving 15 mg pellets of KCl (NIST standard reference material 1655) in water with stirring at 26 °C.

2.3.2. Water adsorption calorimetry

The water adsorption calorimetric experiment was performed in three steps on NMT-2 sample (BET particle size = 99.8 ± 0.4 nm). First, the sample was degassed under vacuum for 12 h at 150 °C to remove all adsorbed water. Second, the free volume of the sample tube and the BET surface areas of the samples were determined using a Micromeritics ASAP 2020. Five point N_2 adsorption isotherms were collected after each degassing or heat treatment. Third, a coupled Micromeritics ASAP2020 analyzer and a Setaram DSC111 Calvet microcalorimeter operated at 25 °C was used to measure the water adsorption enthalpy on the nano calcite surface.

The instrument and methodology are described in greater detail elsewhere (Ushakov and Navrotsky, 2005). Briefly, a pelletized sample (3 mm diameter) taken in one side of a specially designed silica glass fork tube is placed inside the twin chambers of the DSC111 Calvet microcalorimeter and this allows the empty side of the tube to serve as a reference. This tube placed inside the calorimeter is plugged into the analysis port of Micromeritics ASAP2020 analyzer. Water vapor was introduced into the forked tube in incremental values of ~1 micromoles H_2O per dose using ASAP2020 analyzer. The amount of adsorbed water vapor on the sample surface in forktube was determined from the pressure drop (relative pressure P/P_0) as the water vapor is removed from the sample chamber onto the sample surface. The corresponding heat of adsorption of water vapor for each incremental addition was measured by the DSC111 Calvet microcalorimeter operated by 'Calisto acquisition' software. Each water dose generates a distinct calorimetric peak and the area under the peak corresponds to heat of adsorption (differential enthalpy of adsorption) of dosed water. The water adsorption experiment was performed twice on fresh NMT-2 sample (Run 1 and Run 2). To determine experimental uncertainties, each run was repeated (Run 1b and Run 1b) with degassing at 150 °C for 6 h between the measurements. A blank (empty tube) was also run but no appreciable amount of water adsorption for the measured experimental relative pressure (P/P_0) range was observed, thus no additional correction to the data was necessary.

3. RESULTS AND DISCUSSION

3.1. Sample characterization

The XRD patterns of the nano- and bulk samples confirmed that all samples were pure calcite (PDF # 60-7239) (Fig. 1). Elemental analysis of the nanophase calcite samples indicates no significant contamination by other alkali or alkali-earth elements (Table 1) and no detectable amounts of organics or amorphous phases were observed with infrared spectroscopy. Magnesium was the largest contaminant, which was found between 0.4 and 1.08 at% for the nanophase samples. Given the similarities between the cation size and charge, magnesium can easily substitute into the calcium sites. Small amounts of potassium and strontium were also observed. The bulk calcite sample contained undetectable amounts of magnesium and 1.61% potassium originating from the K_2CO_3 starting material.

The infrared spectra of the calcite samples contain peaks corresponding to either calcite or water (Fig. 2). Major bands at 713, 875 and 1420 cm^{-1} correspond to the in-plane-bending (v_4), out-of-plane bending (v_2), and the asymmetric stretching (v_3) of the carbonate groups, respectively (Farmer, 1974). The combination bands $v_1 + v_4$, $2v_2 + v_4$, $2v_3$ are also observed at 1797, 2515, and 2875 cm^{-1}, respectively. Diffuse bands associated with bound water are present in the nanophase calcite samples at 3400 cm^{-1}. These bands are noticeably absent from the bulk calcite sample, confirming the results from the TGA and heating experiments. Bands associated with the presence of organic contaminants, i.e. C–H vibrations, and amorphous calcium carbonate, are not observed in the spectra.

Additional heating experiments to quantify the water content indicate that the bulk calcite sample contains no adsorbed water and the nanophase samples contain between 0.9 and 1.3 wt% H_2O (Table 2). X-ray diffraction patterns of the heated samples indicated no observable coarsening when the adsorbed water was removed from the nanophase calcite particles. Even when the samples were heated to partial decomposition, no coarsening of the particles was evident.

Thermogravimetric analysis of the calcite samples indicates that the decomposition temperatures range from 831 to 859 °C (Fig. 3) with onset occurring at approximately 600 °C, as summarized in Table 2. The decomposition temperature of Iceland spar single crystals was previously reported at 850 °C (Rodriguez-Navarro et al., 2009), which is within the range of the values reported here. A study by Yue et al. (1999) found a downward shift in the

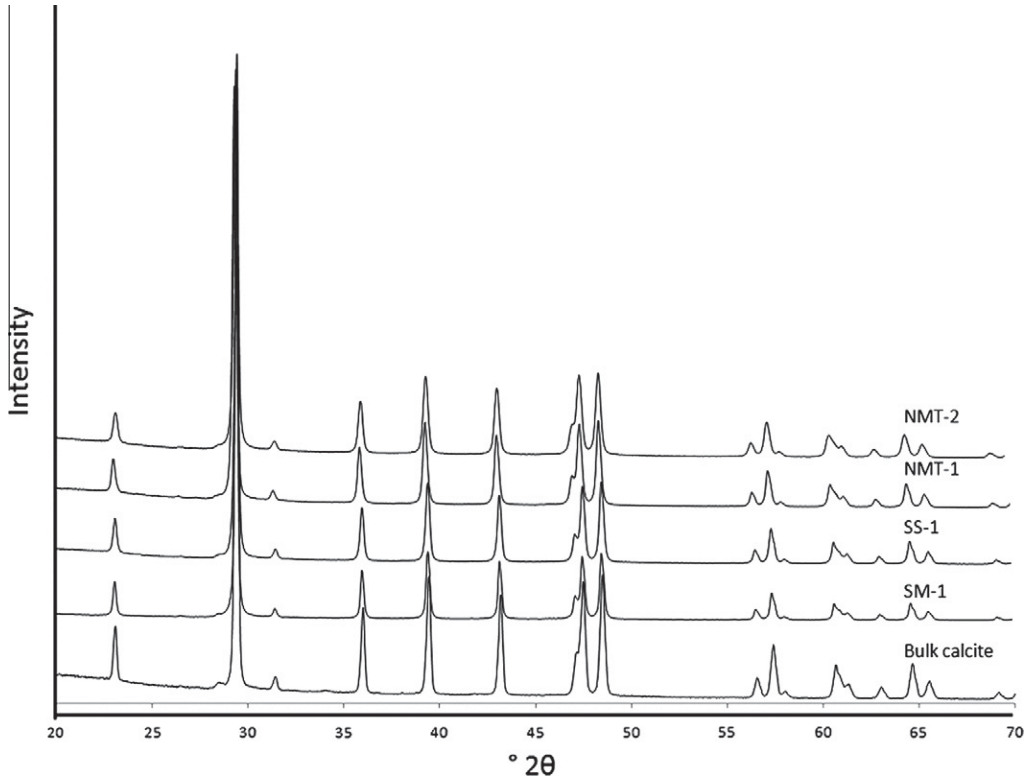

Fig. 1. X-ray diffraction patterns of nanophase and bulk samples, which were identified as calcite (PDF # 60-7239).

Table 1
Elemental analysis (at%) of the nanocalcite phases determined by ICP-MS.

Element	SM-1	SS-1	NMT-1	NMT-2	BCAL
Li	0	0	0	0	0.24 ± 0.01
Na	0	0	0	0	0
Mg	0.4 ± 0.04	1.03 ± 0.08	1.08 ± 0.07	0.93 ± 0.06	0
K	0.11 ± 0.01	0.04 ± 0.02	0.17 ± 0.01	0.11 ± 0.01	1.61 ± 0.07
Sr	0.0136 ± 0.0004	0.017 ± 0.001	0.020 ± 0.001	0.019 ± 0.001	0.70 ± 0.03
Ba	0	0	0	0	0

decomposition temperature (approximately 50 °C) for nanophase calcite compared to the bulk. This shift was not observed in the TGA experiments and no significant trend in the decomposition temperature was found. All nanophase calcite samples decomposed to calcium oxide as confirmed by XRD.

3.2. Particle size analysis

The crystallite size and calculated surface areas (based on whole pattern fitting using the Scherrer Equation (Scherrer, 1918) and assuming spherical particles) are summarized in Table 3. The crystallite size ranges from 28 ± 2 to 74 ± 2 nm for the nanophase calcite samples and greater than 100 nm (limitation of the Scherrer equation) for the bulk sample. The calculated surface areas based on XRD particle sizes range from 2995 ± 80 to 7914 ± 609 m^2/mol [29.92–79.07 m^2/g] for the nanophase calcite samples.

The nitrogen adsorption isotherm for all BET measurements were linear and surface areas measured range from 1321 ± 18 to 2243 ± 9 m^2/mol [13.09–22.17 m^2/g] for the nanophase calcite samples (Table 3). The measured surface areas from BET are smaller than the values obtained from the particle size analysis by XRD, with differences ranging from 36% to 76%. The degassing procedure for removal of adsorbed water was varied (temperature and time), but there was no observable difference in the resulting surface areas. The XRD patterns indicated that no coarsening occurred during the degassing process. Weight loss after degassing also corresponded to the measured water content from the isothermal weight loss studies, indicating that the adsorbed water had been removed completely from the particles.

The particle morphology observed by TEM of all the nanophase samples was rhombohedral and there was little evidence of particle aggregation (Fig. 4). The average particle sizes based on TEM measurements range from 65 ± 2 to

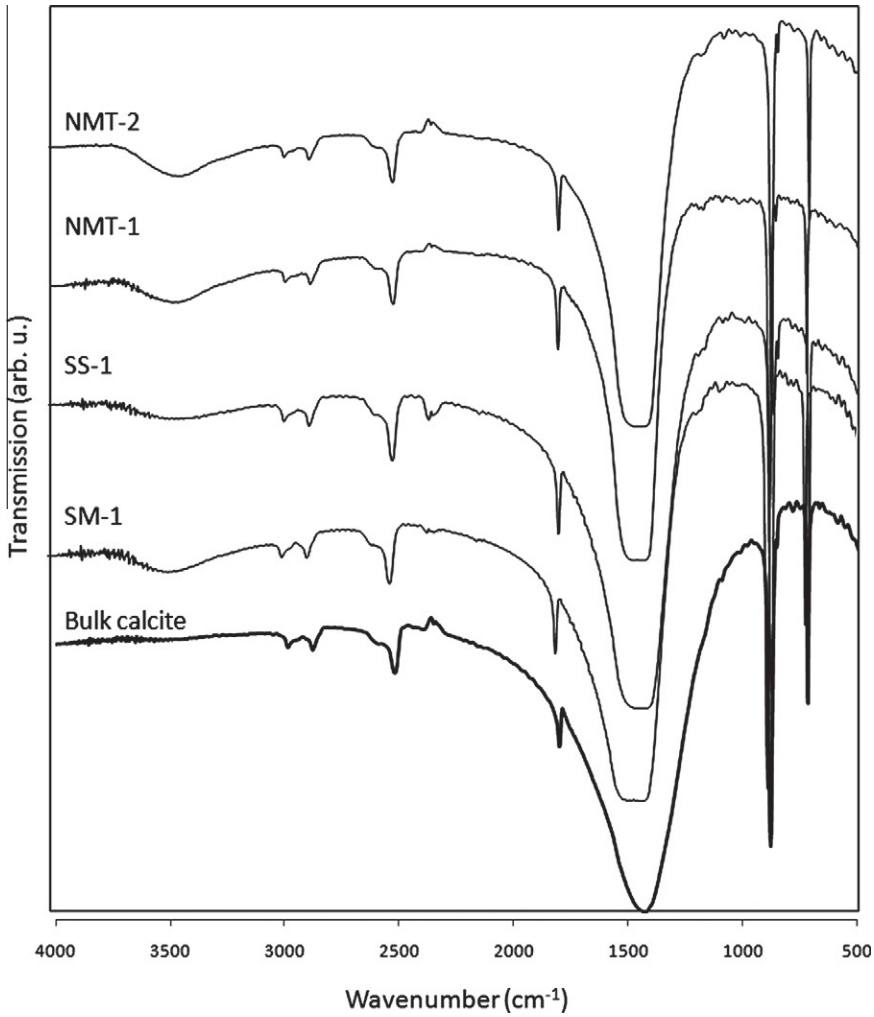

Fig. 2. The infrared spectra of the samples are consistent with pure calcite. A broad band at approximately 3400 cm^{-1} is observed for the nanophase samples, consistent with the presence of approximately 1 wt% H_2O observed during the heating experiments.

Table 2
Decomposition temperature and water content for calcite samples.

Sample	Composition	Decomposition temperature (°C)	H_2O wt%
SM-1	$Ca_{0.996}Mg_{0.004}CO_3 \cdot 0.052\ H_2O$	858	0.92
SS-1	$Ca_{0.99}Mg_{0.01}CO_3 \cdot 0.055\ H_2O$	859	0.98
NMT-1	$Ca_{0.99}Mg_{0.01}CO_3 \cdot 0.038\ H_2O$	831	0.68
NMT-2	$Ca_{0.99}Mg_{0.01}CO_3 \cdot 0.069\ H_2O$	844	1.23
Bulk calcite	$Ca_{0.984}K_{0.016}CO_3$	840	0.00

133 ± 4 nm (Table 3). Again assuming spherical particle, the surface areas for the nanocalcite samples range from 1669 ± 5 to $3409 \pm 10\ m^2/mol$ [16.67–34.06 m^2/g]. Thus, the discrepancy between the BET and TEM measurements are much smaller (10–30%), but are still significant. As the surface area is crucial for the analysis of the calorimetric data, the most accurate method for determining surface area for the nanophase calcite samples had to be determined.

Two major obstacles exist for accurately determining particle size based on analysis of the FWHM of the obtained XRD patterns. First, small changes in the sample height and the anisotropic nature of the material may cause broadening of the diffraction peaks. However these discrepancies are generally accounted for by using a standard to offset instrument effects. Second, the choice of the shape factor (K) used in the Scherrer equation can affect the calculated particle size. Previous studies have shown that the shape factor for calcium carbonate can vary significantly depending on the severity of the particle elongation, in some cases ranging from 1.1 to 2.5 (Jung et al., 2000). Indeed, the surface areas obtained from XRD closely resemble the BET surface areas when a K of 1.4 is assumed. Assigning a K factor is somewhat arbitrary, as it relies upon other methods to assess the accuracy of the results. Thus we regard the particle size and surface area determined by XRD to be of relatively low accuracy.

The morphology is also an issue when estimating particle size and surface area by TEM analysis. Calculating the surface area under the assumption that the particle is a sphere leads to the discrepancy between the BET and

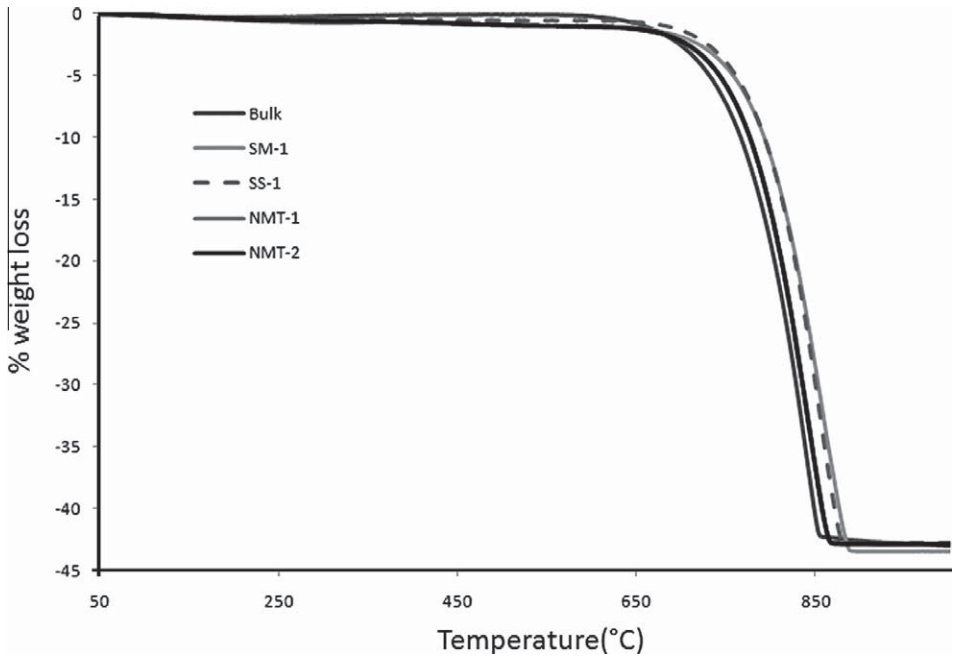

Fig. 3. The thermogravimetric analysis of the calcite samples in air from 30 to 1000 °C. The decomposition to CaO occurs at approximately 850 °C. No significant difference in the decomposition temperature is observed between the nanophase and bulk calcite material.

Table 3
Determination of particle sizes (nm) and surface areas (m^2/mol) by X-ray diffraction, TEM, and BET analysis.

Sample	XRD particle size (nm)	XRD SA (m^2/mol)	TEM particle size (nm)	TEM SA (m^2/mol)	BET particle size (nm)	BET SA (m^2/mol)
SM-1	74 ± 2	2995 ± 80	92 ± 2	2409 ± 10	117.8 ± 1.0	1895 ± 16
SS-1	42 ± 2	5276 ± 260	133 ± 4	1669 ± 5	169.0 ± 2.3	1321 ± 18
NMT-1	36 ± 2	6155 ± 323	119 ± 3	1867 ± 5	150.6 ± 2.6	1488 ± 15
NMT-2	28 ± 2	7914 ± 609	65 ± 2	3409 ± 10	99.8 ± 0.4	2243 ± 9
Bulk calcite	>100		5000	44.3	7000 ± 100	30 ± 4

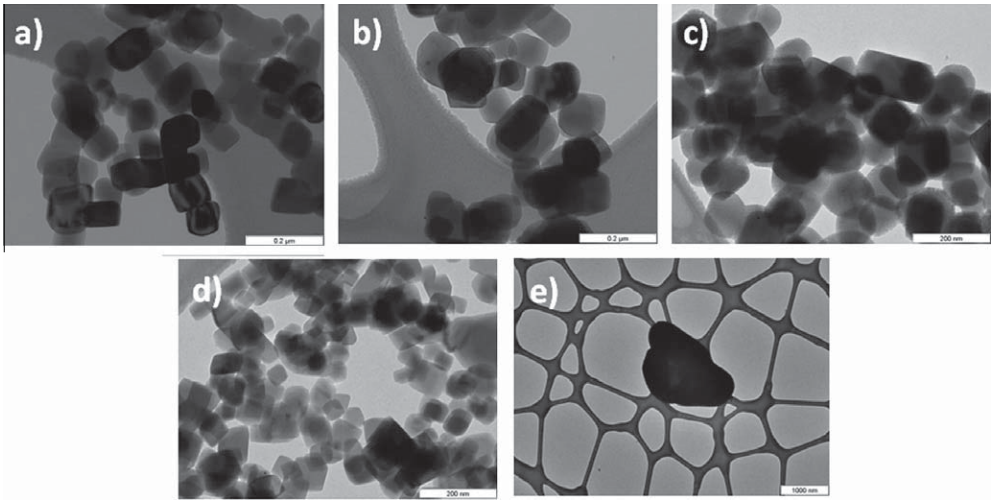

Fig. 4. Representative TEM images for the calcite samples: (a) SM-1, (b) SS-1, (c) NMT-1, (d) NMT-2, (e) bulk calcite. The scale bar represents 200 nm for all nanophase samples and 1000 nm for the bulk calcite image.

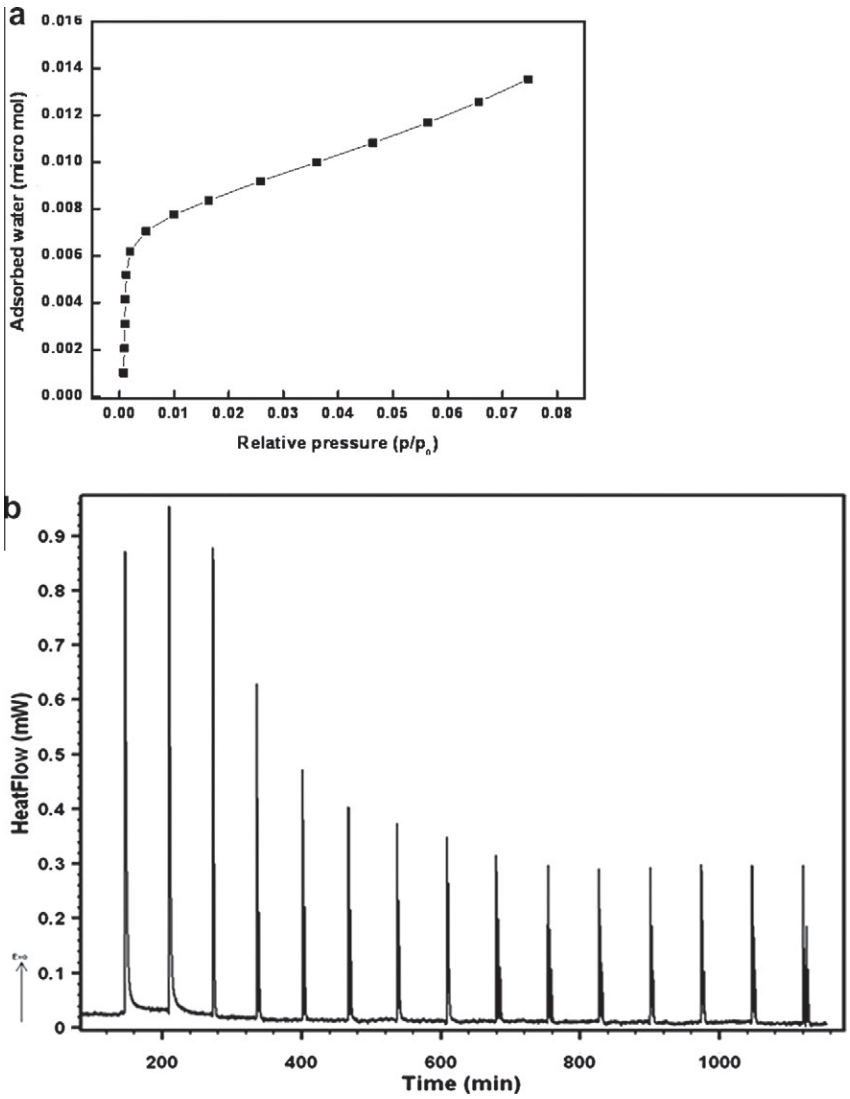

Fig. 5. A typical water adsorption isotherm with corresponding calorimetric peaks for the nanocalcite sample.

TEM surface area values. Identifying the crystallite faces may allow for the estimation of length to width to height ratios and thus a more accurate surface area assessment. If one assumes that the height and width are equal, then the surface area calculated from the TEM images approaches the value obtained from BET analysis. As an example, assuming an equal height and width for particles of the SM-1 sample results in a value of $2174 \pm 50\ m^2/mol$. This value is similar to the surface area obtained by BET ($1895 \pm 16\ m^2/mol$).

Given the limitations of the particle size analysis by XRD and TEM and the absence of obvious aggregation or twinning, we consider the BET analysis the most accurate measurement of the surface area of the nanophase calcite samples. The linear isotherms and lack of coarsening provide additional evidence that the BET surface areas are accurate. Thus the BET surface area values will be used for further analysis of calorimetric data. This has also been done in many of our earlier studies on surface energies of

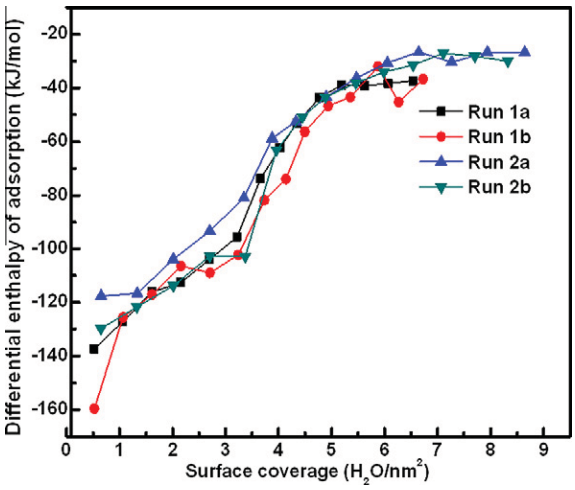

Fig. 6. Differential enthalpies of water adsorption as a function of surface coverage (H_2O per nm^2).

Table 4
Water adsorption calorimetric data.

Sample	Integral enthalpy of adsorption of water vapor (kJ/mol H_2O)	Integral enthalpy of adsorption of liquid water (kJ/mol H_2O)	Coverage H_2O/nm^2	Chemisorbed water (mole) from coverage
Run-1a	−96.87	−52.87	4.78	0.0161
Run-1b	−96.59	−52.59	5.36	0.0180
Run-2a	−86.29	−42.29	4.90	0.0165
Run-2b	−95.31	−51.31	4.88	0.0164
Average (3)	−96.26 ± 0.96	−52.26 ± 0.96	5.01 ± 0.63	0.0168 ± 0.0026

oxides (Levchenko et al., 2006; Mazeina et al., 2006; Park et al., 2010; Zhou et al., 2010).

3.3. Calorimetric measurements

3.3.1. Water adsorption experiments

Nanocalcite samples are generally associated with adsorbed water and the enthalpy of chemisorbed water is determined by the water adsorption calorimetry. Fig. 5 shows a typical water adsorption isotherm and the corresponding calorimetric peaks for the nanocalcite sample degassed at 150 °C. The intensities of calorimetric peaks decrease with successive dosing since the enthalpies of water adsorption (differential enthalpies) become less exothermic. Fig. 6 illustrates the differential enthalpies of water vapor adsorption as a function of surface coverage (H_2O per nm^2). The enthalpies of water adsorption (differential enthalpies) become less exothermic and finally reaches the enthalpy of condensation for bulk water at 25 °C (−44 kJ/mol) after approximately 8–10 doses. The average water coverage value on the sample surface at this point was found to be 5.01 ± 0.63 H_2O/nm^2. The total water adsorbed up to the condensation point can be considered chemisorbed water that is strongly bound to the calcite surface. The remaining water, with a differential enthalpy −44 kJ/mol, can be treated as physically adsorbed water. The integral enthalpy, which is the sum of the differential enthalpies of adsorption divided by the total water up to this coverage, corresponds to the enthalpy of chemisorbed water from the vapor state. The integral enthalpy (ΔH_{ads}) for the surface degassed at 150 °C was found to be −96.26 ± 0.96 kJ/mol. Table 4 gives the summary of the water adsorption calorimetric data. The computed hydration energy value reported from various atomistic simulation techniques range between −79.2 to −138.9 kJ/mol (Liang et al., 1996; de Leeuw and Parker, 1998; Kerisit and Parker, 2004; Rahaman et al., 2008). The enthalpy of water adsorption determined from the water adsorption calorimetric measurements (−96.26 ± 0.96 kJ/mol) falls within the theoretically calculated range.

The ideal monolayer coverage for physically and chemically adsorbed water with cross sectional areas of 0.125 and 0.25 nm^2 would be 8 and 4 H_2O per nm^2, respectively (Brunauer et al., 1956). The average coverage on nanocalcite surface is about 5.01 ± 0.63 H_2O per nm^2 and is close to the chemisorbed water coverage. The differential enthalpies up to 3 H_2O per nm^2 coverage are more exothermic, where as that between 3 and 5.5 H_2O per nm^2 coverage region increases rapidly and reaches a plateau of −44 kJ/mol. This trend in differential enthalpy curves with surface coverage (see Fig. 6) could possibly be due to distinct modes of water adsorption on different active sites on nanocalcite surface. Several molecular dynamic simulation studies on adsorbed water density distribution on calcite surface (Kerisit and Parker, 2004; Rahaman et al., 2008) have also indicated the existence of three different conformational modes for water adsorption on calcite surface. The two modes within the first layer have two hydrogen atoms of the water molecule pointing either up away from the surface or down toward a carbonate ion. The third mode with OH bond of the water pointing straight down towards carbonate ion forms above the second layer (Rahaman et al., 2008). Such active site energetic distribution for water adsorption was also observed in our earlier water adsorption calorimetric study on TiO_2 anatase 3D sea urchin-like assemblies and nano wires (Park et al., 2010).

3.3.2. Solution calorimetry

The enthalpies of solution (ΔH_{sol}) for the calcite samples measured by isothermal acid solution calorimetry at 25 °C are exothermic and range from −25.56 ± 0.41 to −28.67 ± 0.34 kJ/mol (Table 5). The measured enthalpy of solution of the sample includes contributions of adsorbed water, surface enthalpy and the dissolution of nanocalcite phase. The excess enthalpy obtained after subtracting the contributions of water and the bulk phase dissolution from enthalpies of solution (ΔH_{sol}) results in the surface enthalpy for the given surface area.

The calorimetric effect associated with the presence of water on the nanophase calcite samples has been corrected for the physically adsorbed ($\Delta H_{sol\text{-}corr\text{-}physi}$) or chemisorbed ($\Delta H_{sol\text{-}corr\text{-}chemi}$) liquid water. The correction for the hydrous surface is based upon the thermochemical cycle listed in Table 6 and assumes the adsorbed water is a liquid phase that has no chemical interaction with the particle's surface. Little change is observed between the uncorrected (ΔH_{sol}) and corrected values ($\Delta H_{sol\text{-}corr\text{-}physi}$) (Table 5). The correction for chemisorbed liquid water is made by using integral enthalpy (ΔH_{ads}) obtained from the water adsorption calorimetry, with the remainder treated as liquid water. The integral enthalpy (ΔH_{ads}) corresponds to the enthalpy for chemisorption of water from the vapor phase at 25 °C. The enthalpy for chemisorption for liquid water ($\Delta H_{chemiads\text{-}liq}$) was obtained by removing the enthalpy of condensation of water vapor at 25 °C (−44 kJ/mol) from the integral enthalpy ($\Delta H_{chemiads}$). The corrected value ($\Delta H_{sol\text{-}corr\text{-}chemi}$) is based upon the thermochemical cycle given in Table 6 and corresponds to anhydrous surface. The enthalpies for the conversion from nanophase to bulk calcite ($\Delta H_{nano\rightarrow bulk}$) have also been calculated using the thermochemical cycle listed in Table 6. The ranges of

Table 5
The enthalpies of dissolution (ΔH_{sol}), corrected ($\Delta H_{sol\text{-}corr}$) solution, and transition ($\Delta H_{nano\rightarrow bulk}$) enthalpies from nano to bulk obtained by acid solution calorimetry for the nanophase calcite samples.

Sample	ΔH_{sol} (kJ/mol)	$\Delta H_{sol\text{-}corr\text{-}physi}$ (kJ/mol)	$\Delta H_{sol\text{-}corr\text{-}chem}$ (kJ/mol)	$\Delta H_{nano\rightarrow bulk\ \text{-}hydrous}$ (kJ/mol)	$\Delta H_{nano\rightarrow bulk\ \text{-}anhydrous}$ (kJ/mol)
Bulk	-25.56 ± 0.41				
SM-1	-28.67 ± 0.34	-28.65 ± 0.34	-29.47 ± 1.02	-3.09 ± 0.53	-3.91 ± 1.10
SS-1	-27.45 ± 0.29	-27.43 ± 0.29	-28.00 ± 1.00	-1.87 ± 0.5	-2.44 ± 1.08
NMT-1	-27.57 ± 0.37	-27.55 ± 0.29	-28.20 ± 1.03	-1.99 ± 0.55	-2.64 ± 1.11
NMT-2	-28.32 ± 0.56	-28.29 ± 0.29	-29.26 ± 1.11	-2.73 ± 0.69	-3.70 ± 1.18

Table 6
Thermochemical cycles used to calculate the $\Delta H_{sol\text{-}corr\text{-}physi}$, $\Delta H_{sol\text{-}corr\text{-}chem}$ and $\Delta H_{nano\rightarrow bulk}$ for the calcite samples.

Correction for liquid water (hydrous surface)	
$CaCO_3 \cdot nH_2O_{(xl,\ 298\ K)} + 2HCl_{(sln,\ 298\ K)} \rightarrow Ca^{2+}{}_{(sln,\ 298\ K)} + CO_{2(g,\ 298\ K)} + (1+n)H_2O_{(sln,\ 298\ K)} + 2Cl^-{}_{(sln,\ 298\ K)}$	$\Delta H_1 = \Delta H_{sol}$
$H_2O_{(l,\ 298\ K)} \rightarrow H_2O_{(sln,\ 298\ K)}$	$\Delta H_2 = -0.4$ kJ/mol (Parker, 1965)
$CaCO_{3(xl,\ 298\ K)} + 2HCl_{(sln,\ 298\ K)} \rightarrow Ca^{2+}{}_{(sln,\ 298\ K)} + CO_{2(g,\ 298\ K)} + 2Cl^-{}_{(sln,\ 298\ K)} + H_2O_{(sln,\ 298\ K)}$	$\Delta H_4 = \Delta H_{sol\text{-}corr\text{-}physi}$
	$\Delta H_4 = \Delta H_1 - n\Delta H_2$
Correction for chemisorbed liquid water (anhydrous surface)	
$CaCO_3 \cdot nH_2O_{(xl,\ 298\ K)} + 2HCl_{(sln,\ 298\ K)} \rightarrow Ca^{2+}{}_{(sln,\ 298\ K)} + CO_{2(g,\ 298\ K)} + (1+n)H_2O_{(sln,\ 298\ K)} + 2Cl^-{}_{(sln,\ 298\ K)}$	$\Delta H_1 = \Delta H_{sol}$
$H_2O_{(l,\ 298\ K)} \rightarrow H_2O_{(sln,\ 298\ K)}$	$\Delta H_2 = -0.4$ kJ/mol (Parker, 1965)
$H_2O_{(chemi\text{-}ads,\ 298\ K)} \rightarrow H_2O_{(liq,\ 298\ K)}$	$\Delta H_3 = (\Delta H_{chemads\text{-}liq}) = 52.26 \pm 0.96$ kJ/mol
$CaCO_{3(xl,\ 298\ K)} + 2HCl_{(sln,\ 298\ K)} \rightarrow Ca^{2+}{}_{(sln,\ 298\ K)} + CO_{2(g,\ 298\ K)} + 2Cl^-{}_{(sln,\ 298\ K)} + H_2O_{(sln,\ 298\ K)}$	$\Delta H_4 = \Delta H_{sol\text{-}corr\text{-}chem}$
	$\Delta H_4 = \Delta H_1 - n\Delta H_2 - (x)\Delta H_3$
Enthalpy of conversion from nano to bulk	
$CaCO_{3(xl,\ bulk,\ 298\ K)} + 2HCl_{(sln,\ 298\ K)} \rightarrow Ca^{2+}{}_{(sln,\ 298\ K)} + CO_{2(g,\ 298\ K)} + 2Cl^-{}_{(sln,\ 298\ K)} + H_2O_{(sln,\ 298\ K)}$	$\Delta H_5 = \Delta H_{sol\text{-}cor,\ bulk}$
$CaCO_{3(xl,\ nano\ 298\ K)} + 2HCl_{(sln,\ 298\ K)} \rightarrow Ca^{2+}{}_{(sln,\ 298\ K)} + CO_{2(g,\ 298\ K)} + 2Cl^-{}_{(sln,\ 298\ K)} + H_2O_{(sln,\ 298\ K)}$	$\Delta H_6 = \Delta H_{sol\text{-}cor,\ nano}$
$CacO_{3(xl,\ nano,\ 298\ K)} \rightarrow CaCO_{3(xl,\ bulk,\ 298\ K)}$	$\Delta H_7 =$ and $\Delta H_{nano\rightarrow bulk}$ $\Delta H_7 = \Delta H_6 - \Delta H_5$

$\Delta H_{nano\rightarrow bulk}$ for hydrous ($\Delta H_{nano\rightarrow bulk\text{-}hydrous}$) and anhydrous ($\Delta H_{nano\rightarrow bulk\text{-}anhydrous}$) surface are given in Table 5.

3.3.3. Surface enthalpy for the hydrous and anhydrous surface

The difference in the solution enthalpies for the nanophase and bulk calcite samples stems from the increased surface areas of the nanophase samples. This relationship is represented by:

$$\Delta H_{sol\text{-}bulk} = \Delta H_{sol\text{-}corr,\ nano} + SA * \gamma$$

where SA is the surface area of the particle in m^2/mol and γ is the surface enthalpy (J/m^2). The corrected enthalpy values for hydrous ($\Delta H_{sol\text{-}corr\text{-}physi}$) and anhydrous ($\Delta H_{sol\text{-}corr\text{-}chemi}$) surfaces can be plotted against the surface area obtained from BET analysis (Fig. 7a and b). The surface energy of the sample can be determined as the negative of the slope if the relationship is linear. A non-linear trend may be observed if the samples are aggregated, as the excess energy of the sample is now due to both the surface and interface energies (Costa et al., 2010). Straight lines that give R^2 values 0.92 and 0.98 (goodness of the fit) can be fit through the data for hydrous and anhydrous surfaces. The surface enthalpies for hydrous and anhydrous nanocalcite surface are found to be 1.48 ± 0.21 and 1.87 ± 0.13 J/m^2 and the corresponding intercept values (calcite surface area equal to zero) are -25.51 ± 0.32 and -25.51 ± 0.14 kJ/mol. The difference between the hydrated and anhydrous surface is 0.39 J/m^2 which is almost double the value reported by Hackerman and Hall (0.186 J/m^2) for H_2O-calcite system at 25 °C using water adsorption isotherms (Hackerman and Hall, 1958).

The accuracy of the method can be checked by removing the bulk calcite values and calculating the enthalpy of solution based upon the resulting fit of the linear trend line. This changes the intercept from -25.63 to -25.98 kJ/mol and the surface enthalpy to 1.2 ± 0.4 J/m^2 for hydrous surface. The calculated value $\Delta H_{sol\text{-}corr,\ bulk}$ for the bulk calcite with 30 m^2/mol surface area is -26.01 kJ/mol, which is within 0.43 kJ/mol of the measured sample (-25.58 ± 0.41 kJ/mol).

Calorimetry measures the surface enthalpy; however, the surface enthalpy can also be considered the surface energy as the excess volume is expected to be small. Furthermore, the contribution of the surface entropy term ($T\Delta S$) is expected to be small at room temperature and indeed for

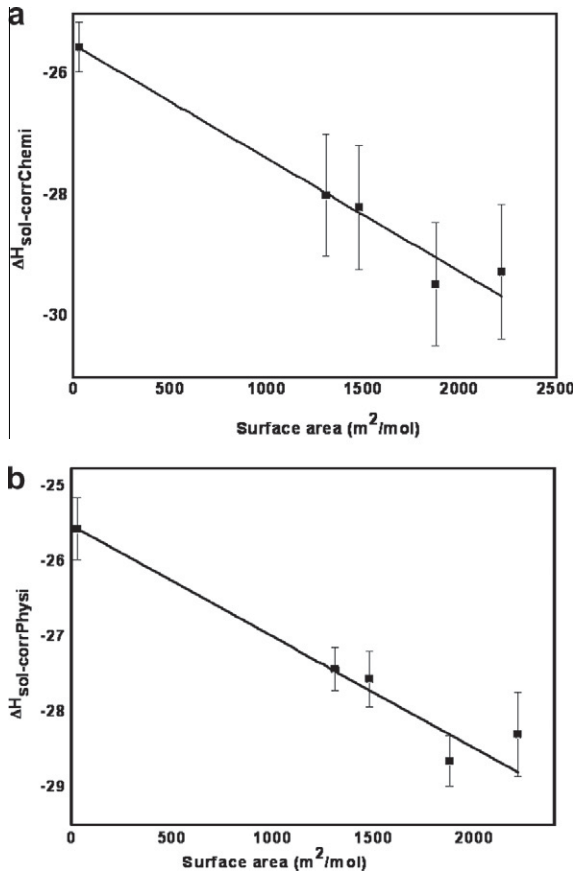

Fig. 7. The solution enthalpies for the (a) hydrous and (b) anhydrous calcite samples plotted against the surface areas obtained by BET analysis. The slope is provides the surface energy of calcite.

TiO_2 the surface entropy itself is found to be negligible (Smith et al., 2009). Based upon the trends observed for oxide minerals, surface enthalpy measured here can be considered an estimate of both the surface energy and surface free energy (surface tension) of calcite.

Several different computational and experimental techniques have been used earlier to evaluate the surface energy of calcite. Most reported values for the surface energy of calcite are based upon computational studies (Supporting information, Tables S1 and S2). These values vary, depending on the modeled crystal face, the surface terminating groups, and the details of the calculation. The {1014} face is the lowest energy face, with relaxed hydrous surface energies ranging from 0.14 to 0.387 J/m^2 (de Leeuw and Parker, 1998; Titloye et al., 1998; Hwang et al., 2001; Kerisit et al., 2003; Duffy and Harding, 2004; Kvamme et al., 2009). Several other higher energy faces have also been modeled with hydrous surface energies ranging from 0.43 to 0.77 J/m^2 (de Leeuw and Parker, 1998; Titloye et al., 1998; Hwang et al., 2001; Braybrook et al., 2002; Kerisit et al., 2003; Duffy and Harding, 2004; Bruno et al., 2008; Massaro et al., 2008; Kvamme et al., 2009). The energy for anhydrous calcite surfaces have also been reported and range from 0.59 to 2.65 J/m^2. The surface energy values obtained by calorimetry for the hydrous and anhydrous surfaces are higher than those obtained from modeling. Generally, calculated surface energy values and those obtained by experiments agree within 10–50% (Navrotsky, 2009). Differences between the two probably arise from the complexity of real surfaces compared to the idealized planar surfaces in most calculations.

Significant scatter of the data is also observed in measured calcite surface energies using different experimental methods (Sohnel and Mullin, 1982; Lioliou et al, 2007; Dousi et al, 2003; Gomez-Morales et al., 2010; Manoli and Dals, 2002; Gilman, 1960; Gupta and Santhananam, 1969; Royne et al, 2011; Janczuk and Bialopiotrowicz, 1986; Okayama, 1997; Goujon and Mtaftschiev, 1976; Wade and Hackerman, 1959) (Supporting Information, Table S2). Most experimentally determined surface energy values for calcite are obtained from homogeneous and heterogeneous nucleation studies. These values are in a very low range (0.032 and 0.085 J/m^2) (Sohnel and Mullin, 1982; Lioliou et al., 2007; Manoli and Dalas, 2002; Dousi et al., 2003), and thus are two orders of magnitude lower than the value obtained by calorimetry. The surface energy is calculated from the induction time of the nucleation experiment. However, the model for both homogeneous and heterogeneous nucleation is based upon classical nucleation theory, where the solid formed at nucleation is assumed to be calcite. As the nucleation pathway of calcite may occur through the initial precipitation of an amorphous calcium carbonate (ACC) precursor, the induction times may not accurately assess the calcite phase. A concern regarding the formation of a precursor phase was raised by Christoffersen et al. (1991) in derivations of the interfacial surface tension of calcite based upon nucleation experiments. The surface energy of such metastable precursor phases (ACC or vaterite) are generally expected to be lower than that of the stable calcite phase.

Other surface energy values for calcite are based upon wettability and contact angle (Janczuk and Bialopiotrowicz, 1986; Okayama et al., 1997). In a study by Okayama et al. (1997) the wetting of calcite surfaces was explored using various methods, wetting liquids and treatments of the calcite surface. The surface energy values were found to be dependent on the type of calcite surface. For example, the freshly-cleaved calcite sample (unknown cleavage plane) had a surface free energy in excess of 0.072 J/m^2 and heating tended to reduce that value. When the freshly cleaved calcite surface was immersed in water, time dependent changes were observed, suggesting that the surface may have undergone restructuring. The surface energy values obtained by heat of immersion technique on calcite surface (surface area = 0.4–2.2 m^2/g) are found to be 0.54–0.76 J/m^2 (Wade and Hackerman, 1959; Goujon and Mtaftschiev, 1976). Balk and Benson (1959) observed that the indirect measurements of surface thermodynamic properties have inherent limitations as they involve the measurement of small differences between large quantities. An additional difference is that these energies refer to calcite totally immersed in water and not to a crystal surface exposed to air (with or without a thin hydration layer).

The values we obtained from calorimetry are higher compared to values reported by different computational

and other experimental techniques. Such differences between the theoretical and calorimetrically measured surface energy values on high surface area particles were also reported for NaCl and KCl (Balk and Benson, 1959). Experimental samples contain a range of surface planes and defect structures that would contribute to a higher surface energy. Additional experimental evidence for higher energy calcite surfaces includes an AFM study by Baltrusaitis and Grassian (2009). They report that a freshly cleaved {1 0 1 4} calcite surface undergoes restructuring when exposed to water vapor at ambient temperature. The study reveals that the surface is heterogeneous with respect to the composition, phases present, and even water content. Further, incorporation of trace elements such as Co^{2+}, Mn^{2+} and Zn^{2+} are shown to induces morphological modification of calcite surface with preferential dopant metal localization on high energy surfaces (Braybrook et al., 2002). These results suggest that simple models may not be adequate to capture the diverse topography of the hydrated surface.

The measured energy for the hydrous calcite surface is similar to those observed in metal oxide systems, though at the lower end of the observed range. For instance, the surface energies for the α- and γ-alumina are 1.7 ± 0.1 and 2.6 ± 0.2 J/m^2 (McHale et al., 1997), and the TiO_2 polymorphs, rutile and anatase, are 2.22 ± 0.07 and 0.74 ± 0.04 J/m^2 (Levchenko et al., 2006). The energies of hydrous surfaces for iron oxide minerals hematite (0.75 ± 0.16 J/m^2) and maghemite (0.57 ± 0.10 J/m^2) (Mazeina and Navrotsky, 2007; Bomati-Miguel et al., 2008) are smaller than the values measured for calcite. The surface enthalpies for oxyhydroxides appear smaller than those for oxides, thus boehmite and goethite values are 0.52 ± 0.12 and 0.60 ± 0.10 J/m^2, respectively (Majzlan et al., 2000; Mazeina and Navrotsky, 2007). For oxides and oxyhydroxides, the order of decreasing surface energies generally follows the increasing metastability of the polymorph (Navrotsky, 2003, 2004). The surface energies for anhydrous oxide surfaces and oxyhydroxides are also similar to those observed with calcite and are higher than the measured values for hydrated surfaces (Mazeina et al., 2006; Mazeina and Navrotsky, 2007; Majzlan et al., 2007).

The anhydrous bulk calcium carbonate polymorphs have small transition enthalpies of −0.92 and −4.35 kJ/mol for the conversion of aragonite and vaterite to calcite, respectively (Plummer and Busenberg, 1982). Computer simulations for aragonite suggest that the surface energy should be in the range 0.16–0.81 and 0.59–1.39 J/m^2 for the hydrous and anhydrous surface, respectively (Aquilano et al., 1997; de Leeuw and Parker, 1998). Vaterite is the most metastable and least dense (2.66 g/cm^3) calcium carbonate phase. The modeled surface energies for vaterite are in the range 0.24–1.15 and 0.62–1.58 J/m^2 for the hydrous and anhydrous surface, respectively (de Leeuw and Parker, 1998). Given the small differences in the transition enthalpy and modeled surface energies of the calcium carbonate polymorphs, an energy crossover from calcite to aragonite and/or vaterite seems possible. Experimental measurements of the surface enthalpies of aragonite and vaterite require well characterized nanophase samples and synthesis is currently being attempted. Interestingly much natural vaterite, appears to be nanophase (Rodriquez-Navarro et al., 2007), supporting the idea of an energy crossover among polymorphs.

4. CONCLUSIONS

Four nanophase and one bulk calcite samples were characterized by XRD, BET, TEM, TGA, IR, and ICP-MS. Our results suggest that particle size determination for calcite sample is best performed using BET analysis. The solution enthalpies of the nanophase samples were found to be more exothermic than that of the bulk. The results from the acid solution and water adsorption calorimetry indicated that the surface energies for hydrous and anhydrous nano calcite are 1.48 ± 0.21 and 1.87 ± 0.16 J/m^2. Given the small differences in energy between the calcium carbonate polymorphs, there is a good possibility that stability crossovers of the nanoscale exist for this system. Future studies will focus on obtaining surface energies for aragonite and vaterite phases. Understanding the energy landscape of these polymorphs will greatly enhance our understanding of calcium carbonate precipitation and success of a geologic repository for carbon dioxide.

ACKNOWLEDGEMENTS

This material is based upon work supported as part of the 'Center of Nanoscale Control of Geologic CO_2', an Energy Frontier Research Center funded by the U.S. Department of Energy, Office of Science, Office of Basic Energy Sciences under Award Number DE-AC02-05CH11231. We would like to thank the following companies for providing the calcite samples for analysis: Specialty Minerals, Inc. Bethlehem, PA, SpringSky Nanomaterials, Houston, TX, NanoMaterials Technology Co., Ltd., Shanxi, China, and NanoMaterials Technology Co., Singapore. The authors would also like to thank Dr. Sergey Ushakov for assistance with the TEM instrument and the water adsorption calorimetry and Joel Commisso for the ICP analysis.

APPENDIX A. SUPPLEMENTARY DATA

Supplementary data associated with this article can be found, in the online version, at doi:10.1016/j.gca.2011.09.034.

REFERENCES

Aquilano D., Rubbo M., Catti M. and Pavese A. (1997) Theoretical equilibrium and growth morphology of $CaCO_3$ polymorphs: I. Aragonite. *J. Cryst. Growth* **182**, 168–184.

Baitalow F., Wolf G. and Schmidt H.-G. (1998) Thermochemical investigations of calcium carbonate phase transitions 1. Thermal activated vaterite-calcite transition. *J. Therm. Anal.* **52**, 5–16.

Balk P. and Benson G. C. (1959) Calorimetric determination of the surface enthalpy of potassium chloride. *J. Phys. Chem.* **63**, 1009–1012.

Baltrusaitis J. and Grassian V. H. (2009) Calcite (1 0 1 4) surface in humid environment. *Surf. Sci.* **17**, L99–L104.

Braybrook A. L., Heywood B. R., Jackson R. A. and Pitt K. (2002) Parallel computational and experimental studies of the morphological modifications of calcium carbonate by cobalt. *J. Cryst. Growth* **243**, 336–344.

Bomati-Miguel O., Mazeina L., Navrotsky A. and Veintemillas-Verdaguer S. (2008) Calorimetric study of maghemite nanoparticles synthesized by laser-induced pyrolysis. *Chem. Mater.* **20**, 591–598.

Brunauer S., Kantro D. L. and Weise C. H. (1956) The surface energy of amorphous silica and hydrous amorphous silica. *Can. J. Chem.* **34**, 1483–1496.

Bruno M., Massaro R. F. and Prencipe M. (2008) Theoretical structure and surface energy of the reconstructed {01.2} form of calcite ($CaCO_3$) crystal. *Surf. Sci.* **602**, 2774–2782.

Christoffersen J., Rostrup E. and Christoffersen M. R. (1991) Relation between interfacial surface tension of electrolyte crystals in aqueous suspension and their solubility; a simple derivation based on surface nucleation. *J. Cryst Growth* **113**, 599–605.

Costa G. C., Ushakov S. V., Castro R., Navrotsky A. and Muccillo R. (2010) Calorimetric measurements of surface and interface enthalpies of yttria stabilized zirconia (YSZ). *Chem. Mater.* **22**, 2937–2945.

de Leeuw N. H. and Parker S. C. (1998) Surface structure and morphology of calcium carbonate polymorphs calcite, aragonite, and vaterite: an atomistic approach. *J. Phys. Chem. B* **102**, 2914–2922.

Dousi E., Kallitsis J., Chrissanthopoulos A., Mangood A. H. and Dalas E. (2003) Calcite overgrowth on carboxylated polymers. *J. Cryst. Growth* **253**, 496–503.

Duffy D. M. and Harding J. H. (2004) Growth of polar crystal surfaces on ionized organic substrates. *Langmuir* **20**(18), 7637–7642.

Farmer V. C. (1974) *The Infrared Spectra of Minerals*. Mineralogical Society, Surrey, UK.

Gebauer D., Volkel A. and Colfen H. (2009) Stable prenucleation calcium carbonate clusters. *Science* **322**, 1819–1822.

Gilman J. J. (1960) Direct measurements of the surface energies of crystals. *J. Appl. Phys.* **31**, 2208–2218.

Gomez-Morales J., Hernandez-Hernandez A., Sazaki G. and Garcia-Ruiz J. M. (2010) Nucleation and polymorphism of calcium carbonate by a vapor diffusion sitting drop crystallization technique. *Cryst. Growth Des.* **10**, 963–969.

Goujon G. and Mtaftschiev B. (1976) On the crystallinity and the stoichiometry of the calcite surface. *J. Colloid Interf. Sci.* **57**, 148–161.

Gupta Y. P. and Santhanam A. T. (1969) On cleavage surface energy of calcite crystals. *Acta Metall.* **17**, 420–424.

Hackerman N. and Hall A. C. (1958) The adsorption of water vapor on quartz and calcite. *J. Phys. Chem.* **62**, 1212–1214.

Han Y. S., Hadiko G., Fuji M. and Takahashi M. (2006) Crystallization and transformation of vaterite at controlled pH. *J. Cryst. Growth* **289**, 269–274.

Hwang S., Blanco M., Demiralp E., Cagin T. and Goddard W. A. (2001) The MS-Q force field for clay minerals: application to oil production. *J. Phys. Chem. B* **105**, 4122–4127.

Janczuk B. and Bialopiotrowicz T. (1986) Spreading of a water drop on a marble surface. *J. Mater. Sci.* **21**, 1151–1154.

Jung W. M., Kang S. H., Kim W.-S. and Choi C. K. (2000) Particle morphology of calcium carbonate precipitated by gas–liquid reaction in a Couette–Taylor reactor. *Chem. Eng. Sci.* **55**, 733–747.

Kerisit S., Parker S. C. and Harding J. H. (2003) Atomistic simulation of the dissociative adsorption of water on calcite surfaces. *J. Phys. Chem. B* **107**, 7676–7682.

Kerisit S. and Parker S. C. (2004) Free energy of adsorption of water and metal ions on the {10.hivin.14} Calcite Surface. *J. Am. Chem. Soc.* **126**, 10152–10161.

Ketzer J. M., Iglesias R., Einloft S., Dullius J., Ligabue R. and de Lima V. (2009) Water–rock–CO_2 interactions in saline aquifers aimed for carbon dioxide storage. Experimental and numerical modeling studies of the Rio Bonito Formation (Permian), southern Brazil. *Appl. Geochem.* **24**, 760–767.

Kharaka Y. K., Thordsen J. J., Hovorka S. D., Nance H. S., Cole D. R., Phelps T. J. and Knauss K. G. (2008) Potential environmental issues of CO_2 storage in deep saline aquifers: geochemical results from the Frio-I Brine Pilot test, Texas, USA. *Appl. Geochem.* **24**, 1106–1112.

Kvamme B., Kuznetsova T. and Uppstad D. (2009) Modelling excess surface energy in dry and wetted calcite systems. *J. Math. Chem.* **46**, 756–762.

Levchenko A. A., Li G., Boerio-Goates J., Woodfield B. F. and Navrotsky A. (2006) TiO_2 stability landscape: polymorphism, surface energy and bound water energetics. *Chem. Mater.* **18**, 6324–6332.

Liang Y., Lea A. S., Baer D. R. and Engelhard M. H. (1996) Structure of the cleaved $CaCO_3$(10.hivin.14) surface in an aqueous environment. *Surf. Sci.* **351**, 172–182.

Lioliou M. G., Paraskeva C. A., Koutsoukos P. G. and Payatakes A. C. (2007) Heterogeneous nucleation and growth of calcium carbonate on calcite and quartz. *J. Colloid Interf. Sci.* **308**, 421–428.

Majzlan J., Navrotsky A. and Casey W. H. (2000) Surface enthalpy of boemite. *Clay. Clay Miner.* **48**(6), 699–707.

Majzlan J., Mazeina L. and Navrotsky A. (2007) Enthalpy of water adsorption and surface enthalpy of lepidocrocite (gamma-FeOOH). *Geochim. Cosmochim. Acta* **71**, 615–623.

Manoli F. and Dalas E. (2002) The crystallization of calcium carbonate on sodium cholate. *J. Mater. Sci. – Mater. Med.* **13**, 69–73.

Massaro F. R., Pastero L., Rubbo M. and Aquilano D. (2008) Theoretical surface morphology of {0112} acute rhombohedron of calcite: a comparison with experiments and {1014} cleavage rhombohedron. *J. Cryst. Growth* **310**, 706–715.

Matter J. M. and Kelemen P. B. (2009) Permanent storage of carbon dioxide in geological reservoirs by mineral carbonation. *Nat. Geo.* **2**, 837–841.

Mazeina L., Deore S. and Navrotsky A. (2006) Energetics of bulk and nano-akaganeite, β-FeOOH: enthalpy of formation, surface enthalpy, and enthalpy of water adsorption. *Chem. Mater.* **18**, 1830–1838.

Mazeina L. and Navrotsky A. (2007) Enthalpy of water adsorption and surface enthalpy of goethite (alpha-FeOOH) and hematite (α-Fe_2O_3). *Chem. Mater.* **19**, 825–833.

McHale J. M., Auroux A., Perrotta A. J. and Navrotsky A. (1997) Surface energies and thermodynamic phase stability in nanocrystalline alumina. *Science* **277**(5327), 788–791.

Meldrum F. C. and Sear R. P. (2009) Now you see them. *Science* **322**, 1802–1803.

Morse W. J., Arvidson R. S. and Luttge A. (2007) Calcium carbonate formation and dissolution. *Chem. Rev.* **107**, 342–381.

Navrotsky A. (2003) Energetics of nanoparticle oxides: interplay between surface energy and polymorphism. *Geochem. Trans.* **4**(6), 34–37.

Navrotsky A. (2004) Energetic clues to pathways to biomineralization: precursors, clusters, and nanoparticles. *Proc. Natl. Acad. Sci.* **101**(33), 12096–12101.

Navrotsky A. (2009) Energetics of oxide nanoparticles. *Int. J. Quant. Chem.* **109**(12), 2648–2657.

Navrotsky A., Mazeina L. and Majzlan J. (2008) Size-driven structural and thermodynamic complexity in iron oxides. *Science* **319**, 1635–1638.

Nebel H. and Epple M. (2008) Continuous preparation of calcite, aragonite, and vaterite, and of magnesium-substituted amorphous calcium carbonate (Mg-ACC). *Z. Anorg. Allg. Chem.* **634**, 1439–1443.

Okayama T., Keller D. S. and Luner P. (1997) The wetting of calcite surfaces. *J. Adhes.* **64**, 231–242.

Park T.-J., Levchenko A. A., Zhou H., Wong S. S. and Navrotsky A. (2010) Shape-dependent surface energetics of nanocrystalline TiO_2. *J. Mater. Chem.* **20**, 8639–8645.

Parker, V. B. (1965) Thermal properties of univalent electrolytes. In *National Standard Reference Data Series* **2**. National Bureau of Standards, 66.

Plummer L. N. and Busenberg E. (1982) The solubilities of calcite, aragonite, and vaterite in CO_2–H_2O solutions between 0 and 90 °C, and an evaluation of the aqueous model for the system $CaCO_3$–CO_2–H_2O. *Geochim. Cosmochim. Acta* **46**, 1011–1040.

Pouget E. M., Bomans P. H. H., Goos J. A. C. M., Frederik P. M., de With G. and Sommerdijk N. A. J. M. (2009) The initial stages of template-controlled $CaCO_3$ formation revealed by cryo-TEM. *Science* **323**, 1455–1458.

Radha A. V., Forbes T. Z., Killian C. E., Gilbert P. U. P. A. and Navrotsky A. (2010) Transformation and crystallization energetics of synthetic and biogenic amorphous calcium carbonate. *Proc. Natl. Acad. Sci.* **107**(38), 16438–16443.

Rahaman A., Grassian V. H. and Margulis C. J. (2008) Dynamics of water adsorption onto a calcite surface as a function of relative humidity. *J. Phys. Chem. C* **112**, 2109–2115.

Ranade M. R., Navrotsky A., Zhang H. Z., Banfield J. F., Elder S. H., Zaban A., Borse P. H., Kulkarni S. K., Doran G. S. and Whitfield H. J. (2002) Energetics of nanocrystalline TiO_2. *Proc. Natl. Acad. Sci.* **99**, 6476–6481.

Rodriguez-Navarro C., Ruiz-Agudo E., Luque A., Rodriguez-Navarro A. B. and Ortega-Huertas M. (2009) Thermal decomposition of calcite: mechanisms of formation and textural evolution of CaO naocrystals. *Am. Miner.* **94**, 578–593.

Rodriquez-Navarro C., Jimenez-Lopez C., Rodriquez-Navarro A., Gonzalez-Munoz M. T. and Rodriquez-Gallego M. (2007) Bacterially mediated mineralization of vaterite. *Geochem. Cosmochem. Acta* **71**, 1197–1213.

Royne A., Bisschop J. and Dysthe D. K. (2011) Experimental investigation of surface energy and subcritical crack growth in calcite. *J. Geophys. Res.* **116**, B04204–B04214.

Scherrer Paul. (1918) Bestimmung der grösse und der inneren struktur von kolloidteilchen mittels röntgenstrahlen. *Nachr. Ges. Wiss. Göttingen* **26**, 98–100.

Smith Stacey. J., Stevens R., Liu S., Li G., Navrotsky A., Boerio-Goates J. and Woodfield B. (2009) Heat capacities and thermodynamic functions of TiO_2 anatase and rutile: analysis of phase stability. *Am. Mineral.* **94**, 236–243.

Sohnel O. and Mullin J. W. (1982) Precipitation of calcium carbonate. *J. Cryst. Growth* **60**, 239–250.

Titloye J. O., de Leeuw N. H. and Parker S. C. (1998) Atomistic simulation of the differences between calcite and dolomite surfaces. *Geochim. Cosmochim. Acta* **62**(15), 2637–2641.

Ushakov S. V. and Navrotsky A. (2005) Direct measurements of water adsorption enthalpy on hafnia and zirconia. *Appl. Phys. Lett.* **87**, 164103/1–164103/3.

Wade W. and Hackerman N. (1959) Heats of immersion II. Calcite and kaolinite – Effect of pretreatment. *J. Phys. Chem.* **63**, 1639–1641.

Wolf G., Konigsberger E., Schmidt H.-G., Konigsberger L.-C. and Gamsjager H. (2000) Thermodynamic aspects of the vaterite-calcite phase transition. *J. Therm. Anal. Calorim.* **60**, 463–472.

Wolf G., Lercher J., Schmidt H.-G., Gamsjager H., Konigsberger E. and Schmidt P. (1996) Thermodynamics of $CaCO_3$ phase transitions. *J. Therm. Anal.* **46**, 353–359.

Wray J. L. and Daniels F. (1957) Precipitation of calcite and aragonite. *J. Am. Chem. Soc.* **79**(9), 2031–2034.

Yue L., Shui M. and Xu Z. (1999) The decomposition kinetics of nanocrystalline calcite. *Thermochim. Acta* **335**, 121–126.

Zhou W., Ushakov S. V., Wang T., Ekerdt J. G., Demkov A. A. and Navrotsky A. (2010) Hafnia: energetics of thin films and nanoparticles. *J. Appl. Phys.* **107**, 123514–123517.

Associate editor: Jacques Schott